

Electrochemical corrosion behaviors of aluminum-based marine coatings in the presence of *Escherichia coli* bacterial biofilm



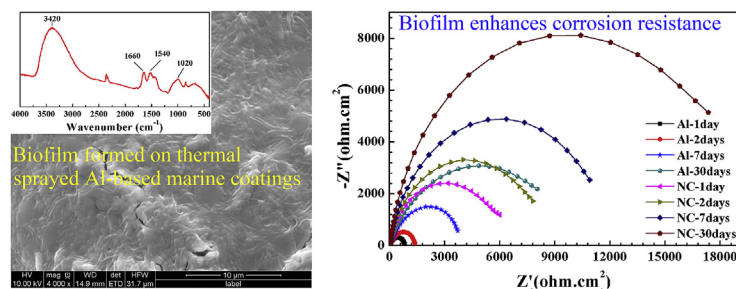
Leila Abdoli, Jing Huang, Hua Li*

Key Laboratory of Marine Materials and Related Technologies, Zhejiang Key Laboratory of Marine Materials and Protective Technologies, Ningbo Institute of Materials Technology and Engineering, Chinese Academy of Sciences, Ningbo, 315201, China

HIGHLIGHTS

- Biocorrosion behavior of thermal sprayed Al and Al/nano- Al_2O_3 coatings was studied.
- A biofilm was formed on the coating surfaces after colonization of the bacteria.
- The biofilm enhances corrosion resistance of the Al-based coatings in early stages.
- Equivalent circuit models were proposed to elucidate the biocorrosion mechanisms.

GRAPHICAL ABSTRACT



ARTICLE INFO

Article history:

Received 2 August 2015
Received in revised form
31 October 2015
Accepted 13 January 2016
Available online 5 February 2016

Keywords:

Coatings
Electrochemical techniques
Corrosion
Electrochemical properties

ABSTRACT

Corrosion behavior of thermal sprayed Al and Al/nano- Al_2O_3 composite coatings in artificial seawater in the presence of *Escherichia coli* bacteria were investigated. A biofilm has been built-up on the coating surfaces following the colonization of the bacteria after 7 days soaking in the solution. The bacteria-related biofilm was used as the simplified model for examining the anti-biocorrosion performances of the marine coatings. The biofilm enhances the corrosion resistance of the Al-based coatings in early stages. Simulated results using equivalent circuit models provide direct electrochemical information about the liquid/surface interfaces, further elucidating the anti-biocorrosion mechanisms of the coatings.

© 2016 Elsevier B.V. All rights reserved.

1. Introduction

Corrosion is one of the persistent problems for marine infrastructures, which occurs due to chemical or electrochemical reactions between the marine environment and metals. Presence of microorganism in the corrosive media makes the corrosion more complicated. For most metallic materials for instance stainless steel

316L [1] used in the marine environment, their mechanical, physical and chemical properties can be damaged by the activity of the microorganisms that attach on the surfaces of the metallic structures. Colonization of microorganisms on metallic surface is capable of changing the electrochemical reaction at biofilm/metal interface, in turn either inhibiting or accelerating the corrosion [2,3]. Use of thermal spray technique has been successful for effectively protecting the marine structures from corrosion through providing inorganic coatings for maintenance-free long-term services [4–8]. Thermal spray process offers the advantages of cost-efficiency, wide selection of coating materials, and easy on-site

* Corresponding author.

E-mail address: lihua@nimte.ac.cn (H. Li).

operation, making it one of the most promising surface coating techniques. Due to the intrinsic feature of the technique, the coatings usually exhibit high levels of interlamellar cracks and micropores, which could be detrimental to corrosion resistance [9]. Development of biofilm on the surfaces of the coatings would certainly influence their anti-corrosion properties. In-depth knowledge has been gained pertaining to the biocorrosion of metallic alloys. However, unfortunately, there are so far few reports available elucidating the biocorrosion behavior of thermal sprayed marine coatings. Related knowledge is still lacking.

Surface properties of the marine structures certainly affect the bacteria attachment. Some materials enhance the formation of bacteria biofilm while some inhibit bacterial growth. It was reported that under identical environmental conditions, *Bacillus mycoides* accelerated corrosion of zinc, inhibited corrosion of aluminum, and showed no effect on the corrosion of mild steel [10]. Surface roughness, polarization, oxide coverage, and chemical composition have remarkable impact on bacterial attachment and biofilm formation [11]. Eashwar et al. [12] proposed that the ennoblement of stainless steels in seawater was caused by the inhibitors produced by bacteria retained in biofilm matrix. Further evidence that bacteria may be beneficial has been reported [13,14]. It was found that the protective biofilms decreased the corrosion rate of steels by reducing oxygen concentration at the metal surfaces [15–19]. The positive effect attained by biofilms on anti-corrosion performances have also been realized for other metals such as brass and copper [20,21]. However, in many cases the same bacteria with inhibitory property may also become aggressive [22], which leads to the well-known biocorrosion. The corrosion rate is completely different depending on the presence/absence of the biofilm. Yet precise evaluation and discrimination between usual corrosion and microbially influenced corrosion has been very hard, since the involvement of microorganisms would be always very delicate and difficult to be fixed [23–26].

Among the thermal sprayed marine coatings, aluminum coatings have proven to perform well in the marine environment. However, in many cases, use of aluminum coatings is limited since marine corrosion always accompanies wear. In recent years, nanostructured coatings have attracted significant attention due to their promise of significantly optimized or enhanced properties. It is generally believed that, because of their ultrafine structures, the coatings with nanostructures possess novel properties compared to traditional materials and have opened up opportunities for new technological applications [27–29]. The inhibited corrosion by biofilm is usually believed to be predominately attributed to removal of corrosion agents, formation of a protective layer, elimination of corrosion-causing bacteria by antimicrobial agent, production of peptide corrosion inhibitor, or production of biosurfactant. Whereas formation of oxygen concentration cell, generation of corrosive substances, alternation of electrolyte ion concentration, and bacteria-induced inactivation of corrosion inhibitor are the likely mechanisms of accelerated corrosion by microorganisms [22]. Influence of the biofilm formed on the surfaces of thermal sprayed inorganic coatings on their corrosion behavior yet keeps elusive. In this study, the corrosion behavior of thermal sprayed Al and Al/nano- Al_2O_3 coatings with a biofilm formed on their surfaces in artificial seawater were examined. The biofilm constructed mainly by *Escherichia coli* (*E. coli*) bacteria was employed as the simplified model for the investigation. The biocorrosion mechanism of the coatings was further elucidated by microstructure characterization and modeling the liquid/metal interfaces.

2. Materials and methods

2.1. Fabrication of the coatings

Stainless steel 316L plates with the dimension of $20 \times 20 \times 2$ mm were used as the substrates. The steel was composed of 0.029wt.% C, 0.075wt.% N, 0.71wt.% Si, 0.035wt.% P, 2.04wt.% Mo, 0.02wt.% S, 15.92wt.% Cr, 1.41wt.% Mn, 11.35wt.% Ni and remaining iron. Prior to the spraying, the substrates were degreased ultrasonically in acetone followed by grit blasting using 60 mesh black fused alumina sand. Commercially available Al powder with the size range of 50–100 μm was used as the starting feedstock. For the composite coating deposition, the starting Al/nano- Al_2O_3 powder was prepared by ball milling of the Al powder and 30 nm Al_2O_3 powder (Jingrui New Material Co., Ltd, China) for 30 min at 300 rpm. The ball to powder weight ratio was 10:1. For each milling pot, 10 g of the powder with an Al/nano- Al_2O_3 weight ratio of 9:1 was pre-mixed mechanically. The coatings were deposited using both high velocity arc spray (AS, TLAS-500C, China) and plasma spray (APS-2000K, China). For the arc spraying, the current and voltage of the arc were 100 A and 25 V respectively, and the spray distance was 150 mm. The compressed air with the pressure of 0.5 MPa was used as auxiliary gas. The plasma spraying was conducted with the net energy of 25 kW and spray distance of 120 mm. The feed rate of the powder was 20 g/min carried by argon gas with the flow rate of 4 l/min. The flow rate of the primary gas argon and the secondary gas hydrogen was 42 l/min and 12 l/min respectively. The thickness of the coatings was $\sim 200 \mu\text{m}$.

2.2. Characterization and corrosion testing of the coatings

Microstructure of the powder and the coatings was characterized by field emission scanning electron microscope (FESEM, FEI Quanta FEG 250, the Netherlands). After exposed for different immersion time, 2, 7, and 30 days, in sterile and inoculated medium containing *E. coli*, the samples were examined by SEM to get their surface characteristics and corrosion features. To immobilize the bacterial cells, the samples were immersed for 4 h in 2.5% glutaraldehyde solution. Then the samples were dehydrated by using four ethanol solutions of 25%, 50%, 75% and 100% successively for 15 min each. Energy-dispersive X-ray spectroscopy (EDX) detection was also performed to analyze the chemical compositions at local surface regions of the samples. For the corrosion testing of the coatings, potentiodynamic polarization and electrochemical impedance spectroscopy (EIS) spectra were acquired using a Solartron Modulab system (2100A, UK). All the testing was conducted at room temperature in artificial seawater (ASW) prepared according to the ASTM D1141-98 (2003). Peptone with the concentration of 3 g/l was added to the media as carbon and energy sources for the bacteria. The medium was adjusted to the pH value of 7 and autoclaved at 121 °C for 20 min. Before the electrochemical measurement, the coating samples were immersed in ASW contained in an aerobic chamber under sterile conditions and in the presence of bacteria. The samples were then incubated at 30 °C in a shaker at 120 rpm at different exposure duration to a maximum of 30 days. Each set of the experiments was repeated three times to ensure reproducibility. A traditional three-electrode cell was used, with 1 cm^2 platinum as the counter electrode, a saturated calomel electrode (SCE) as the reference electrode and the specimen with an exposed area of 1 cm^2 as the working electrode. The surfaces were also sterilized with UV illumination and 70% ethanol for 1 h. EIS measurement was performed with an applied AC signal of 10 mV and the frequency ranging from 100 kHz to 0.01 Hz. After the measurement, the acquired data were fitted and analyzed using a ZSimpWin software based on equivalent circuit models. The

equivalent circuits were chosen based on the number of time constants and the quality of the fits [30,31]. Potentiodynamic polarization curves were acquired with the potential range of -500 mV to 500 mV [32] versus E_{ocp} at a scan rate of 0.5 mVs $^{-1}$.

2.3. Preparation of bacterial strains and characterization of biofilm

Gram-negative *E. coli* bacteria (ATCC No. 25922) were selected for making the simplified biofilm model. The *E. coli* biofilm is typically composed of a thick exopolysaccharide layer, with a structure resembling that of *Pseudomonas* biofilms [33,34]. The bacteria were grown in LB media. The medium was prepared by dissolving 10 g NaCl, 5 g yeast extract and 10 g peptone in 1000 ml deionized water. The media containing the bacterial strains were shaken at 120 rpm for 24 h at 37 °C. Cell number was determined based on the standard calibration with the assumption that an OD_{600nm} value of 1.0 is equivalent to 10^9 cells/ml. The inoculated medium was prepared by adding *E. coli* for an initial concentration of 10^6 cells/ml at 30 °C under aerobic conditions. The biofilm formed on the surfaces of the coatings was characterized by Fourier transformed infrared spectroscopy (FTIR, Nicolet 6700, Thermo Fisher Scientific, USA) with the resolution of 4 cm $^{-1}$ and a scan range of 4000 – 400 cm $^{-1}$.

3. Results and discussion

Topographical morphology of the ball-milled powder is shown in Fig. 1. The Al/nano- Al_2O_3 particles exhibit irregular shapes with the size of ~ 100 μm (Fig. 1a). It is clear that after the ball-milling, the nano- Al_2O_3 particles are attaching on the outmost shell of the Al particles (Fig. 1b). Phase analysis by X-ray diffraction evidenced non

changes in structure of both the Al and the Al_2O_3 after the ball-milling processing (data not shown). Dense coatings were fabricated by the arc/plasma spray, as suggested by their cross-sectional morphologies (Fig. 1c, d). Unique distribution of the nano Al_2O_3 particles is clearly seen from the cross-sectional view of the composite coating (Fig. 1d). This is not surprising since formation of thermal sprayed coating is accumulating process of individual particles. For the starting ball-milled Al/nano- Al_2O_3 powder, the nano alumina particles exist on the surfaces of Al particles. After the coating deposition, the nano particles should be predominately distributed at the interfaces between individual Al splats. The presence of the nano Al_2O_3 particles at Al splats' interfaces should affect the properties that are related to interfacial characteristics of interconnected splats.

It is noted that after 7 days exposure in the inoculated solution, the coatings incubated in the bacteria-free ASW show non changes on their surfaces (Fig. 2 a-1, b-1). While for the coatings immersed for two days in the bacteria-containing ASW, the colonization of *E. coli* bacteria on the coatings are clearly seen (Fig. 2 a-2, b-2). It is noted that the bacterial adhesion initially occurred near the microsized pores and cracks on the surfaces of the coatings. Subsequent accumulation and further growth of the bacteria was resulted predominately surrounding these areas. Secreted extracellular polymeric substances (EPS) are typically seen in the periplasmic space of the bacteria (Fig. 2 b-3), which usually acts as a binding material for the adhesion of bacterial cells to biofilm matrix [35]. The appearance of EPS was also evidenced by EDX analysis in this work (Fig. 3). Generally a thin film with the thickness of ~ 20 – 80 nm forms as the first stage, presumably due to the deposition of inorganic ions and high relative molecular mass organic compounds. This film is able to alter the electrostatic charges and

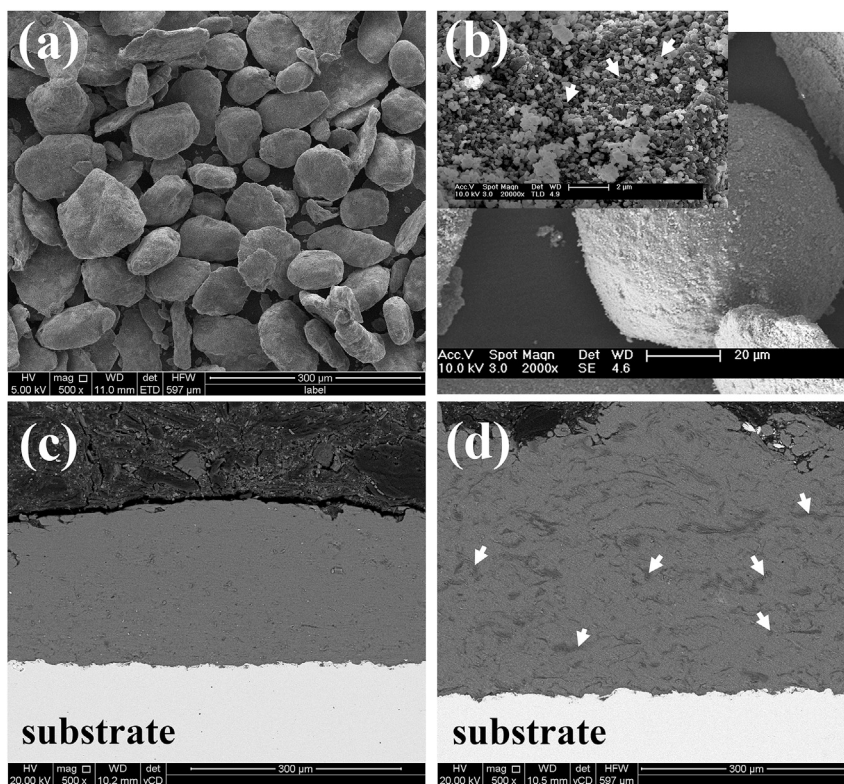


Fig. 1. Typical FESEM morphologies of the ball-milled powder and the coatings, (a) topographical SEM morphology of the milled Al/nano- Al_2O_3 powder, (b) surface view of the ball-milled Al/nano- Al_2O_3 particle showing the nano Al_2O_3 particles attaching on the surface of Al, the inset is enlarged view of selected area of the particle showing the nano sized Al_2O_3 particles, (c) cross-sectional morphology of the Al coating, and (d) cross-sectional morphology of the Al/nano- Al_2O_3 coating. The white arrows point to typical nano Al_2O_3 particles present on the surface of Al particle in (b) and located at the Al splats' interfaces in the coating in (d).

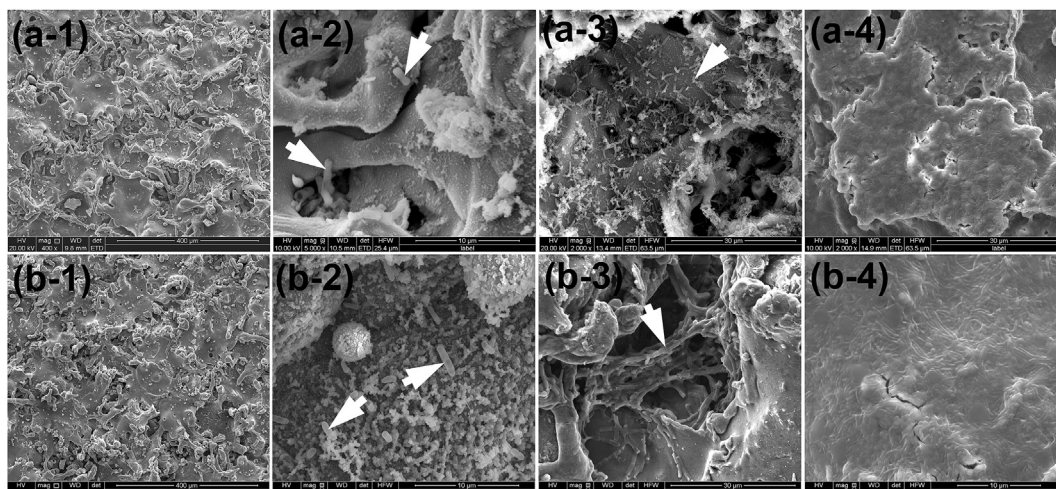


Fig. 2. Surface morphologies of the Al coatings (a) and the Al/nano- Al_2O_3 coatings (b) after being soaked in ASW with/without *E. coli* bacteria. (a-1, b-1) the samples were soaked in the bacteria-free ASW, (a-2, b-2) the samples show clear attachment of the bacteria after 2 days incubation in the bacteria-containing ASW, (a-3, b-3) the samples show clear colonization of the bacteria after 7 days incubation in the bacteria-containing ASW, and (a-4, b-4) the coatings exhibit clearly complete coverage of a biofilm on the their surfaces after 30 days soaking in the bacteria-containing ASW. The white arrow points to typical individual bacterium or interconnected bacteria.

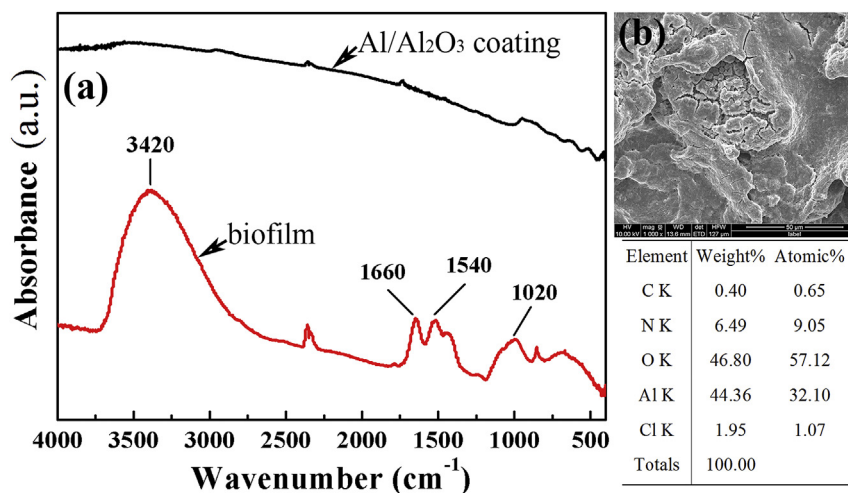


Fig. 3. FTIR spectra (a) and EDX analysis (b) of the biofilm formed on the surfaces of the coatings. For comparison, the IR spectrum was also acquired from the surface of the as-sprayed Al/nano- Al_2O_3 coating. And the EDX detection was made on the overall surface area shown in (b).

wettability of the metal surface, in turn facilitating colonization by bacteria on the surface [36]. EPS usually comprises a wide variety of organic compounds including proteins, polysaccharides, humic acid substances, lipid, DNAs, and so on [37]. Soon after the formation of the film, the microbial growth and EPS production result in the development of a biofilm. However, even though the bacteria have been interconnected in some areas in particular those close to the pores (Fig. 2 b-3), the bacteria-related biofilm is not homogeneous. Further elongated soaking of the coating samples in the bacteria-containing ASW resulted in the formation of continuous biofilm on their surfaces (Fig. 2 a-4, b-4). 30 days immersion of the samples already gave rise to full coverage of the surfaces of the coatings by a homogeneous biofilm. While shorter incubation duration only resulted in uncontinuous localized colonization of the bacteria. The biofilm was further characterized by EDX analysis and FTIR detection (Fig. 3). For comparison purpose, the Al/nano- Al_2O_3 composite coating was also characterized by FTIR (Fig. 3a). The appearance of Al in the biofilm as detected by EDX (Fig. 3b) might suggest dissolution of Al during the incubation, since metal

binding by EPS involves interaction between metal ions and anionic functional groups (e.g. carboxyl, phosphate, sulfate, glycerate, pyruvate and succinate groups) that are common as the protein and carbohydrate components of exopolymers [38]. However, no other metal ions were detected in the biofilm, suggesting the major components of the biofilm as the bacteria and EPS. The IR spectrum for the biofilm shown in Fig. 3a reveals a strong absorption peak at $\sim 3420\text{ cm}^{-1}$ reflecting stretching vibrations of O–H (the functional group in polysaccharides and proteins) and $\sim 1020\text{ cm}^{-1}$ assigned to $-\text{CO}-$ stretching (glycopeptides, ribose). The IR band located at 1660 cm^{-1} refers to C=O and C–N (Amide I) stretching, and the peak at 1540 cm^{-1} reflects combination of N–H bending and C–N (Amide II) stretching (Amide I and Amide II corresponded to the functional groups in proteins) [37,39]. Nevertheless, extensive understanding of the biofilm is essential for clarifying the biofouling behavior of the coatings. Further characterization of the biofilm is required. In addition, only limited information is currently available on the correlation between the physical characteristics of substrate materials and biofilm formation. Among the surface properties of

the materials, surface roughness is believed to be an important factor affecting the formation and composition of the biofilm [40]. Rough surface favors bacterial attachment [41]. In this case, the inherently rough surfaces of the thermal sprayed Al coatings are further roughened by the Al_2O_3 particles added in the coatings [42]. This probably contributes in part to the formation of the more homogeneous biofilm on the composite surface.

The effect of the biofilm on the electrochemical corrosion performances of the coatings was investigated. Electrochemical impedance measurements suggest the positive effect brought about by the bacteria-associated biofilm on corrosion resistance of the coatings (Fig. 4b). For comparison purposes, the corrosion behavior of the coatings soaked in the ASW without the bacteria were initially assessed (Fig. 4 and Fig. S1 in the Supplemental Data). Since it has been realized that one month incubation already resulted in formation of homogeneous biofilm on the surfaces of the coatings, obviously the biofilm significantly enhanced the impedance value of the coatings (Fig. 4 a-2 vs. a-1, and b-2 vs. b-1). It is found that the electrochemical impedance value increases as the incubation time of the coating samples in the solution is prolonged, predominantly due to formation of a passive layer on the coating surfaces. The composite coating with the addition of nano Al_2O_3 shows better corrosion resistance than the pure Al coating in both the testing environments (Fig. 4 b vs. a). It is likely that the Al_2O_3 nanoparticles incorporated into the coatings act as insulators on the surfaces of the coatings. Similar results have also been realized for micron-sized Al_2O_3 particles-incorporated Al coatings [43]. The enhanced anti-corrosion performances are consistent with other reports that degradation of the coatings even at long immersion time is alleviated in the presence of the nanoparticles [44,45]. This could be explained by the strengthened resistance of the coatings by the nano Al_2O_3 particles against hydrolytic degradation and corrosive electrolyte diffusion [44]. During the corrosion testing, the small size and large surface area of the nanoparticles certainly result in decrease in the number of transport paths for corrosive electrolyte diffusion through the coating. In fact, the

nanoparticles could significantly enhance the barrier properties of the coating.

Bacterial adhesion to a surface is a complicated process, which is affected by various physicochemical properties of both bacterial cells and substratum surfaces [46]. The electrochemical testing data shows that as the immersion time increases, the low frequency arc becomes more important and the corrosion resistance increases. SEM characterization already disclosed that the bacterial adhesion occurred near the flaws located on the surfaces of the coatings (Fig. 2 b-3), from where biofilm started to form. The Nyquist spectra for the coatings in the two testing media show two time constants (Fig. 4). Based on the EIS results, as well as the electrochemical studies proposed by Szczygiel et al. [47] on composite coatings containing Al_2O_3 , an EIS equivalent circuit for the coatings is proposed, as shown in Fig. 5. The equivalent circuit models take into account the contribution of various phenomena, such as electrical double layer, biofilm formation, laminar coating structure and others. For the coating samples incubated in the bacteria-containing ASW for 30 days, the model differs from the one describing the samples incubated for 7 days (Fig. 5 b versus a). For the samples incubated for 30 days, apart from a passive film and the double layer, a continuous dense biofilm was readily formed on the coating surfaces for both the Al and the Al/nano- Al_2O_3 composite coatings.

According to the proposed models, the calculated parameters relevant to the impedance results are listed in Table 1. $R_{ct}Q_{dl}$ describes the electrode Faraday process (corrosion process) and corresponds to low-frequency impedance, while the circuit $R_{coat}Q_{coat}$ represents the processes blocking the coating surface and corresponds to high-frequency impedance. The higher frequency time constant is related to the solution/coating interface, and the lower frequency time constant is related to the solution/substrate interface. It is noted that the impedance value increases for all the coating samples after 30 days incubation. This can be well explained since it is likely that protective film or stabilized pre-existing protective film can be easily resulted on metal surface

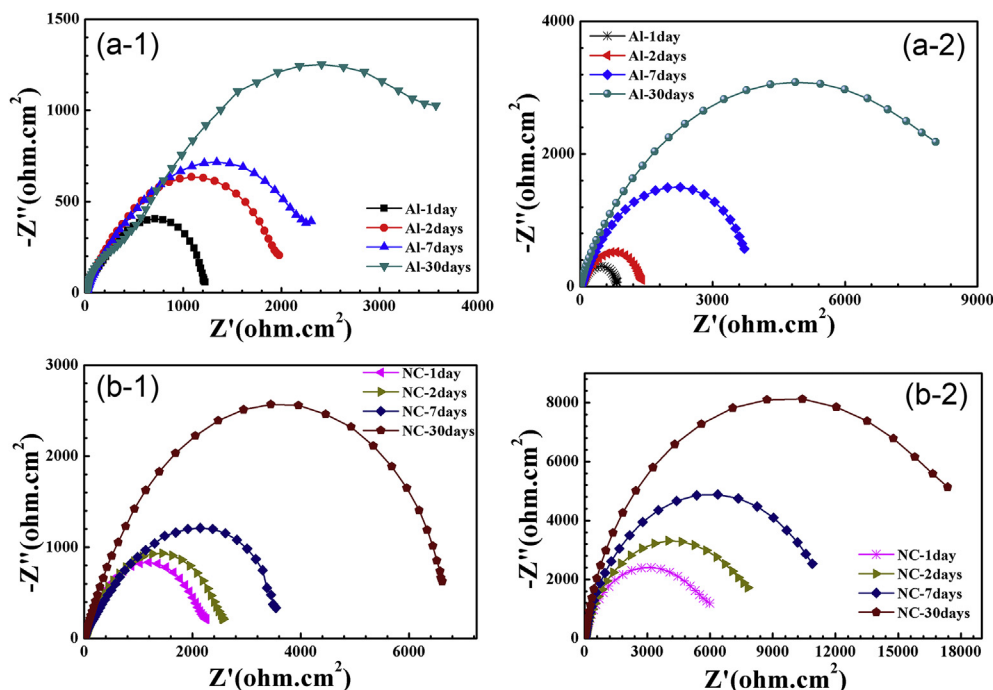


Fig. 4. Nyquist plots for the Al (a) and the Al/nano- Al_2O_3 (b) coating samples incubated in the ASW without (a-1, b-1) or with (a-2, b-2) the bacteria tested with different immersion duration at 30 °C. Al: aluminum coating, NC: Al/nano- Al_2O_3 composite coating.

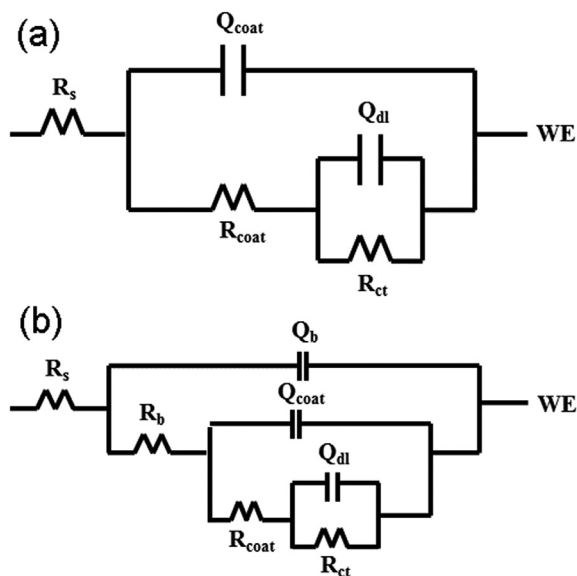


Fig. 5. Schematic equivalent circuit models simulating the experimental impedance diagrams for the coatings soaked in the ASW in absence (a) or presence (b) of *E. coli* after 30 days incubation. R_s : solution resistance, Q_b : capacitance of the biofilm, R_b : biofilm resistance, Q_{coat} : capacitance of the coatings, R_{coat} : resistance of the coatings, Q_{dl} : capacitance of the double layer, R_{ct} : charge transfer resistance.

which could be accounted for by the fine structure nature of the composite coating and the role of the Al_2O_3 nanoparticles as insulators staying on the coating surfaces. It therefore indicates that in presence of the *E. coli*, the bacteria opt to attach on the surface of the coatings, in turn forming the biofilm. The biofilm acts as a protective layer in the corrosive environment. In absence of the bacteria, the corrosive liquid penetrates relatively easily through the coating.

Further potentiodynamic polarization examination for the coatings incubated in the ASW with/without the bacteria suggests consistent results with those suggested by the electrochemical analyses (Fig. 6). In the presence of the bacteria, the corrosion potentials of the coatings shift negatively, but corrosion current densities drop at both exposure times. As expected from the EIS results, the corrosion current density I_{corr} for the Al/nano- Al_2O_3 composite coating is lower than that for the pure Al coating regardless of presence or absence of the bacteria. In the presence of the bacteria, both the anodic and the cathodic curves shift to the left and the anodic and cathodic currents were decreased after 7 days and 30 days. The corrosion current density is lower for the bacteria-containing solution than in the pure ASW solution. As discussed in previous section, the decreased I_{corr} after incubation of the coatings in the solutions is probably attributed to the formation of the bacteria-associated biofilm and the possible oxide layer formed on the surfaces of the coatings. These layers act as barrier protecting

Table 1

Electrochemical impedance parameters obtained from the best fitting of the experimental impedance data determined by using ZSimpWin program.

Sample	R_s $\Omega \cdot cm^2$	R_{ct} $\Omega \cdot cm^2$	R_{coat} $\Omega \cdot cm^2$	R_b $\Omega \cdot cm^2$	CPE_{CT} $\mu F \cdot cm^{-2}$	CPE_{coat} $\mu F \cdot cm^{-2}$	CPE_b $\mu F \cdot cm^{-2}$
Sterile ASW							
-Al coating							
After 1 day	8.494	953.3	289.5	—	445.3	128.4	—
After 2 days	7.973	1812	269.4	—	365.6	122.2	—
After 7 days	17.79	2316	258.6	—	401.5	129.1	—
After 30 days	16.23	4134	461.4	—	521.4	62.64	—
-Al- Al_2O_3 coating							
After 1 day	8.564	2260	93.51	—	69.4	192.4	—
After 2 days	8.068	2294	415.5	—	63.6	200.5	—
After 7 days	8.961	3328	498.6	—	198.5	76.21	—
After 30 days	16.81	5881	1083	—	50.32	85.74	—
ASW with <i>E. coli</i>							
-Al coating							
After 1 day	8.603	634.4	215.8	—	272.3	320.1	—
After 2 days	17.64	1180	241.7	—	305.6	293.4	—
After 7 days	17.66	3710	461.8	—	148.7	252.7	—
After 30 days	8.255	10,290	2987	8.271	120.3	168.8	53.38
-Al- Al_2O_3 coating							
After 1 day	9.602	6261	45.02	—	70.25	166.2	—
After 2 days	10.72	8457	40.74	—	82.14	150	—
After 7 days	14.49	12,030	36.33	—	98.12	117.3	—
After 30 days	10.77	19,690	40.68	26.77	64.82	100.8	102.1

[36]. The simulated EIS results also suggest enhanced corrosion impedances of the coatings with increased exposure time. In this case, the charge transfer resistance, R_{ct} , for the composite coating is higher than that for the pure Al coating. The highly increased R_{ct} value implies high corrosion resistance. For both the coatings, a significant shift in R_{ct} with exposure time was observed. This shift is presumably due to the formation of the biofilm and stabilized pre-existing protective film, which is evidenced by the better corrosion resistance exhibited by the samples than the samples incubated in the ASW without the bacteria. After 30 days, the R_{ct} for the Al and the composite coatings in presence of the bacteria reaches 10,290 $\Omega \cdot cm^2$ and 19,690 $\Omega \cdot cm^2$, respectively. Moreover, the R_{ct} of the composite coating remains higher than that of the Al coating,

the coatings from penetration of aggressive solutions, giving rise to the enhanced corrosion resistance. The electrochemical corrosion variables, namely corrosion potential, E_{corr} , corrosion current density, I_{corr} , anodic Tafel slope, b_a , and cathodic Tafel slope, b_c , are listed in Table 2. The extrapolation of anodic and cathodic Tafel lines gives the corrosion current density at the corrosion potential; and it should start 50–100 mV away from E_{corr} [48]. However, Mansfeld [49] proposed that when the accurate Tafel slopes are not available, they could be determined from the pre-Tafel region in the vicinity of E_{corr} . In this work, the cathodic and anodic branches don't show Tafel behavior in the range of 50–100 mV; so the regions of the cathodic and anodic branches were selected in the range of 30–40 mV. The corrosion current density of the composite coatings

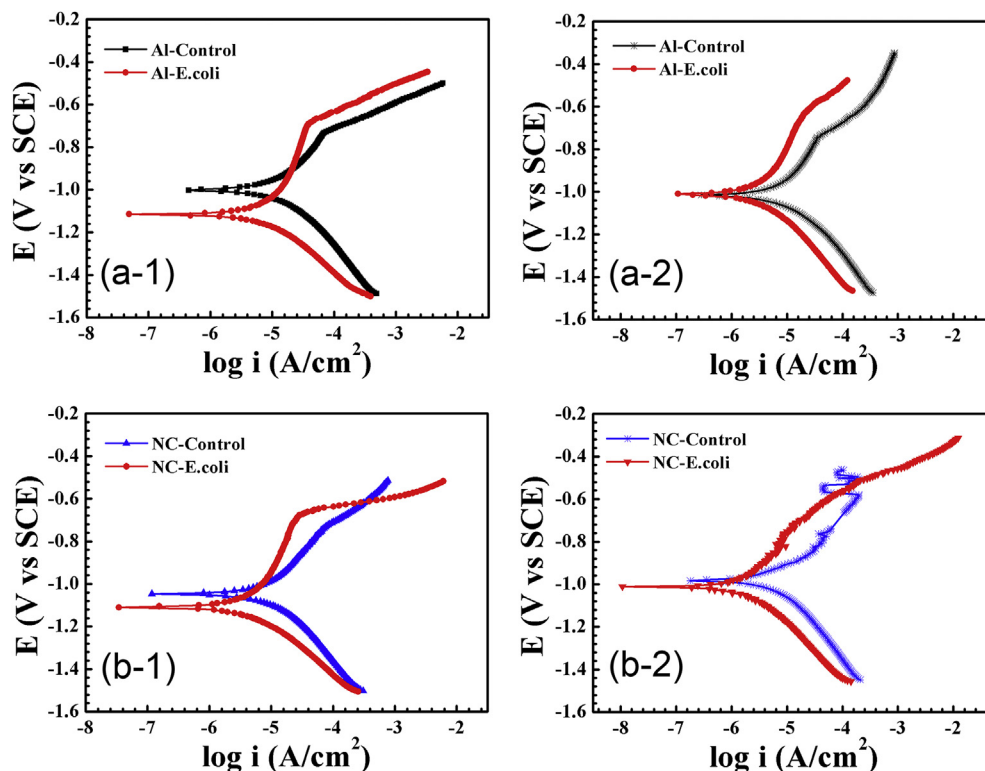


Fig. 6. Potentiodynamic polarization curves of the Al and the Al/nano- Al_2O_3 coatings in the ASW with and without the bacteria after 7 days (a-1, b-1) and 30 days (a-2, b-2) of exposure. Al-control: the Al coating in the ASW without the bacteria, Al-E. coli: the Al coating in the ASW with the bacteria, NC-control: the Al/nano- Al_2O_3 coating in the ASW without the bacteria, NC-E. coli: the Al/nano- Al_2O_3 coating in the ASW with the bacteria.

Table 2
Polarization parameters of the coatings incubated in the sterile ASW and the E. coli-containing ASW.

Sample	E_{corr} (V vs SCE)	I_{corr} ($\mu\text{A}/\text{cm}^2$)	β_c (mV/decade)	β_a (mV/decade)
After 7 days				
Al coating in sterile ASW	-1.006	3.84	-74.82	104.4
Al coating in <i>E.coli</i> -containing ASW	-1.126	2.347	-68.83	137.3
Al- Al_2O_3 coating in sterile ASW	-1.045	2.659	-91.18	94.42
Al- Al_2O_3 coating in <i>E.coli</i> -containing ASW	-1.104	1.076	-80.82	81.18
After 30 days				
Al coating in sterile ASW	-1.017	2.771	-102	129.7
Al coating in <i>E.coli</i> -containing ASW	-1.009	1.1	-112.3	117.7
Al- Al_2O_3 coating in sterile ASW	-0.983	2.396	-122.2	141.7
Al- Al_2O_3 coating in <i>E.coli</i> -containing ASW	-1.011	0.788	-114.9	154.7

in presence of *E. coli* after 30 days incubation is $0.788 \mu\text{A}/\text{cm}^2$, much lower than that of the Al coating, $1.1 \mu\text{A}/\text{cm}^2$, indicating better anti-corrosion performances of the composite coatings.

Formation of Al_2O_3 passive film is likely after the immersion of the Al-based coatings in the ASW, which can be explained by the following reaction: $2\text{Al} + 3\text{H}_2\text{O} \rightarrow \text{Al}_2\text{O}_3 + 6\text{H}^+ + 6\text{e}^-$. Al_2O_3 film is not stable in water and tends to change to $\text{Al}(\text{OH})_3$. Accumulation of the oxide/hydroxide film on the electrode surface diminishes dissolution of Al. Presence of chloride easily triggers breakdown of this film by the interaction between $\text{Al}(\text{OH})_3$ film and Cl^- ions, which produces AlCl_3 after sufficiently long time [50,51]. Formation of biofilm in presence of the bacteria probably stabilizes the oxide layer and in turn prevents the failure of the film. The FESEM images of the coatings after the Tafel polarization testing showed clearly the damaged oxide layer, resulting in occurrence of pitting (data not shown). In fact, presence of chloride has been detected by EDX within the damaged oxide layer (Fig. 3b). Furthermore, the decreased values of I_{corr} and increased R_{ct} also indicate enhanced

passivation of the Al coating by the addition of nano Al_2O_3 particles, which needs to be further investigated.

4. Conclusions

The simplified biofilm model constituted by *E. coli* bacteria and the bacteria-associated secretions was employed for investigating the corrosion behavior of thermal sprayed Al and Al/nano- Al_2O_3 coatings in artificial seawater. Colonization of the bacteria on the surfaces of the coatings was followed by accumulation formation of a homogeneous biofilm. Electrochemical testing revealed significantly enhanced corrosion resistance of the coatings after full homogeneous coverage of the biofilm. The results shed some light on future elucidating the biocorrosion of thermal sprayed inorganic marine coatings and in turn provide insight into design of their microstructures for enhanced properties.

Acknowledgments

This research was supported by National Natural Science Foundation of China (grant # 41476064 and 31271017), Ningbo Municipal Natural Science Foundation (Grant # 2015A610019).

Appendix A. Supplementary data

Supplementary data related to this article can be found at <http://dx.doi.org/10.1016/j.matchemphys.2016.01.038>.

References

- [1] B.J. Little, J.S. Lee, *Microbiologically Influenced Corrosion*, John Wiley & Sons Inc., New Jersey, 2007.
- [2] N.O. San, H. Nazir, G. Donmez, Evaluation of microbiologically influenced corrosion inhibition on Ni–Co alloy coatings by *Aeromonas salmonicida* and *Clavibacter michiganensis*, *Corros. Sci.* 65 (2012) 113–118.
- [3] P.J. Antony, Sh. Chongdar, P. Kumar, R. Ramana, Corrosion of 2205 duplex stainless steel in chloride medium containing sulfate-reducing bacteria, *Electrochim. Acta* 52 (2007) 3985–3994.
- [4] H. Katayama, S. Kuroda, Long-term atmospheric corrosion properties of thermally sprayed Zn, Al and Zn–Al coatings exposed in a coastal area, *Corros. Sci.* 76 (2013) 35–41.
- [5] D. Chaliampalias, G. Vourlias, E. Pavlidou, G. Stergioudis, S. Skolianos, K. Chrissafis, High temperature oxidation and corrosion in marine environments of thermal spray deposited coatings, *Appl. Surf. Sci.* 255 (2008) 3104–3111.
- [6] W. Tian, Y. Wang, T. Zhang, Y. Yang, Sliding wear and electrochemical corrosion behavior of plasma sprayed nanocomposite Al_2O_3 –13% TiO_2 coatings, *Mater. Chem. Phys.* 118 (2009) 37–45.
- [7] J. Kawakita, S. Kuroda, T. Fukushima, T. Kodama, Corrosion resistance of HVOF sprayed HastelloyC nickel base alloy in seawater, *Corros. Sci.* 45 (2003) 2819–2835.
- [8] X. Zhao, D. Yan, S. Li, C. Lu, The effect of heat treatment on the electrochemical corrosion behavior of reactive plasma-sprayed TiN coatings, *Appl. Surf. Sci.* 257 (2011) 10078–10083.
- [9] R. Molins, B. Normand, G. Rannou, B. Hannyoy, H. Liao, Interlamellar boundary characterization in Ni-based alloy thermally sprayed coating, *Mat. Sci. Eng. A-Struct.* 351 (2003) 325–333.
- [10] E. Juzeliunas, R. Ramanaukas, A. Lugauskas, K. Leinartas, M. Samulevicene, A. Sudavicius, Influence of wild strain *Bacillus mycoides* on metals: from corrosion acceleration to environmentally friendly protection, *Electrochim. Acta* 51 (2006) 6085–6090.
- [11] F.M. AlAbbas, J.R. Spear, A.E. Kakpovbia, N.M. Balhareth, D.L. Olson, B.M. Mishra, Bacterial attachment to metal substrate and its effects on microbiologically-influenced corrosion in transporting hydrocarbon pipelines, *J. Pipeline Eng.* 11 (2012) 63–72.
- [12] M. Eashwar, S. Maruthamutu, S. Sathyanarayanan, K. Balakrishnan, The ennoblement of stainless alloys by marine biofilms: the neutral pH and passivity enhancement model, *Corros. Sci.* 37 (1995) 1169–1176.
- [13] A. Pedersen, M. Hermansson, The effects on metal corrosion by *Serratia marcescens* and a *Pseudomonas* sp S9, *Biofouling* 1 (1989) 313–322.
- [14] A. Pedersen, M. Hermansson, Inhibition of metal corrosion by bacteria, *Biofouling* 3 (1991) 1–11.
- [15] C.O. Obuekwe, D.W.S. Westlake, J.A. Plambeck, Evidence that available energy is a limiting factor in the bacterial corrosion of mild steel by a *Pseudomonas* sp. *Can. J. Microbiol.* 33 (1987) 272–275.
- [16] J.S. Potekhina, Inhibition of corrosion on mild steel using aerobic microorganisms, *Prot. Met.* 3 (1984) 469–470.
- [17] A. Jayaraman, E.T. Cheng, J.C. Earthman, T.K. Wood, Axenic aerobic biofilms inhibit corrosion of SAE 1018 steel through oxygen depletion, *Appl. Microbiol. Biot.* 48 (1997) 11–17.
- [18] A. Jayaraman, E.T. Cheng, J.C. Earthman, T.K. Wood, Importance of biofilm formation for corrosion inhibition of SAE 1018 steel by axenic aerobic biofilms, *J. Ind. Microbiol. Biot.* 18 (1997) 396–401.
- [19] A. Jayaraman, J.C. Earthman, T.K. Wood, Corrosion inhibition by aerobic biofilms on SAE 1018 steel, *Appl. Microbiol. Biot.* 47 (1997) 62–68.
- [20] D. Ornek, T.K. Wood, C.H. Hsu, F. Mansfeld, Corrosion control using regenerative biofilms (CCURB) on brass in different media, *Corros. Sci.* 44 (2002) 2291–2302.
- [21] A. Jayaraman, D. Ornek, D.A. Duarte, C.C. Lee, F.B. Mansfeld, T.K. Wood, Axenic aerobic biofilms inhibit corrosion of copper and aluminum, *Appl. Microbiol. Biot.* 52 (1999) 787–790.
- [22] K.A. Zarasvand, V.R. Rai, Microorganisms: induction and inhibition of corrosion in metals, *Int. Biodeter. Biodegr.* 87 (2014) 66–74.
- [23] C. Cote, O. Rosas, M. Sztyler, J. Doma, I. Beech, R. Basseguy, Corrosion of low carbon steel by microorganisms from the 'pigging' operation debris in water injection pipelines, *Bioelectrochemistry* 97 (2014) 97–109.
- [24] Y. El Mendili, A. Abdelouas, H. El Hajj, J.F. Bardeau, Phase transitions of iron sulphides formed by steel microbial corrosion, *RSC Adv.* 3 (2013) 26343–26351.
- [25] H. Kanematsu, H. Ikigai, M. Yoshitake, Evaluation of various metallic coatings on steel to mitigate biofilm formation, *Int. J. Mol. Sci.* 10 (2009) 559–571.
- [26] E. Huttunen-Saarivirta, M. Honkanen, T. Lepisto, V.T. Kuokkala, L. Koivisto, C.G. Berg, Microbiologically influenced corrosion (MIC) in stainless steel heat exchanger, *Appl. Surf. Sci.* 258 (2012) 6512–6526.
- [27] A.K. Basak, S. Achanta, J.P. Celis, M. Vardavoulis, P. Matteazzi, Structure and mechanical properties of plasma sprayed nanostructured alumina and FeCuAl-alumina cermet coatings, *Surf. Coat. Tech.* 202 (2008) 2368–2373.
- [28] Y. Le, P. Hou, J. Wang, J.F. Chen, Controlled release active antimicrobial corrosion coatings with Ag/SiO₂ core-shell nanoparticles, *Mater. Chem. Phys.* 120 (2010) 351–355.
- [29] M.A. Deyab, S.T. Keera, Effect of nano-TiO₂ particles size on the corrosion resistance of alkyd coating, *Mater. Chem. Phys.* 146 (2014) 406–411.
- [30] X.D. He, X.M. Shi, Self-repairing coating for corrosion protection of aluminum alloys, *Prog. Org. Coat.* 65 (2009) 37–43.
- [31] R.Z. Zand, K. Verbeken, A. Adriaens, Electrochemical assessment of the self-healing properties of cerium doped sol-gel coatings on 304L stainless steel substrates, *Int. J. Electrochem. Sci.* 7 (2012) 9592–9608.
- [32] S. Bera, T.K. Rout, G. Udayabhanu, R. Narayan, Comparative study of corrosion protection of sol-gel coatings with different organic functionality of Al-2024 substrate, *Prog. Org. Coat.* 88 (2015) 293–303.
- [33] P.N. Danese, L.A. Pratt, R. Kolter, Exopolysaccharide production is required for development of *Escherichia coli* K12 biofilm architecture, *J. Bacteriol.* 182 (2000) 3593–3596.
- [34] G. O'Toole, H.B. Kaplan, R. Kolter, Biofilm formation as microbial development, *Annu. Rev. Microbiol.* 54 (2000) 49–79.
- [35] Th.M. Ph. Nguyen, X. Sheng, Y. Ting, S.O. Pehkonen, Biocorrosion of AISI 304 stainless steel by *Desulfo* *Wibrio* desulfuricans in seawater, *Ind. Eng. Chem. Res.* 47 (2008) 4703–4711.
- [36] H.A. Videla, Biocorrosion and biofouling of metals and alloys of industrial usage. Present state of the art at the beginning of the new millennium, *Rev. Metal. Madr. Vol. Extr.* (2003) 256–264.
- [37] G. Long, P. Zhu, Y. Shen, M. Tong, Influence of extracellular polymeric substances (EPS) on the deposition kinetics of bacteria, *Environ. Sci. Technol.* 43 (2009) 2308–2314.
- [38] I.B. Beech, J. Sunner, Biocorrosion: towards understanding interactions between biofilms and metals, *Curr. Opin. Biotech.* 15 (2004) 181–186.
- [39] Z. Filip, S. Hermann, An attempt to differentiate *Pseudomonas* spp. and other soil bacteria by FT-IR spectroscopy, *Eur. J. Soil Biol.* 37 (2001) 137–143.
- [40] A. Kerr, M. Cowling, The effects of surface topography on the accumulation of biofouling, *Phil. Mag.* 83 (2003) 2779–2795.
- [41] B. Li, B.E. Logan, Bacterial adhesion to glass and metal-oxide surfaces, *Colloid Surf. B* 36 (2004) 81–90.
- [42] H.S. Grewal, H. Singh, A. Agrawal, Microstructural and mechanical characterization of thermal sprayed nickel-alumina composite coatings, *Surf. Coat. Technol.* 216 (2013) 78–92.
- [43] J. Huang, Y. Liu, J. Yuan, H. Li, Al/Al₂O₃ composite coating deposited by flame spraying for marine applications: alumina skeleton enhances anti-corrosion and wear performances, *J. Therm. Spray Technol.* 23 (2014) 676–683.
- [44] S. Sharifi Golrua, M.M. Attara, B. Ramezanzadeh, Studying the influence of nano-Al₂O₃ particles on the corrosion performance and hydrolytic degradation resistance of an epoxy/polyamide coating on AA-1050, *Prog. Org. Coat.* 77 (2014) 1391–1399.
- [45] B. Ramezanzadeh, M.M. Attar, M. Farzam, A study on the anticorrosion performance of the epoxy-polyamide nanocomposites containing ZnO nanoparticles, *Prog. Org. Coat.* 72 (2011) 410–422.
- [46] S. Bayoudh, A. Othmane, L. Ponsonnet, H.B. Ouada, Electrical detection and characterization of bacterial adhesion using electrochemical impedance spectroscopy-based flow chamber, *Colloid Surf. A* 318 (2008) 291–300.
- [47] B. Szczygiel, M. Kolodziej, Composite Ni/Al₂O₃ coatings and their corrosion resistance, *Electrochim. Acta* 50 (2005) 4188–4195.
- [48] E. Poorgasemi, O. Abootalebi, M. Peikari, F. Haqdar, Investigating accuracy of the Tafel extrapolation method in HCl solutions, *Corros. Sci.* 51 (2009) 1043–1054.
- [49] F. Mansfeld, Tafel slopes and corrosion rates obtained in the pre-Tafel region of polarization curves, *Corros. Sci.* 47 (2005) 3178–3186.
- [50] T. Kaewmaneekul, G. Lothongkum, Effect of aluminium on the passivation of zinc-aluminium alloys in artificial seawater at 80°C, *Corros. Sci.* 66 (2013) 67–77.
- [51] S.I. Pyun, S.M. Moon, S.H. Ahn, S.S. Kim, Effects of Cl⁻, NO₃⁻ and SO₄²⁻ ions on anodic dissolution of pure aluminium in alkaline solution, *Corros. Sci.* 41 (1999) 653–667.